

## Validation of RADARSAT-2 fully polarimetric SAR measurements of ocean surface waves

Biao Zhang,<sup>1</sup> Will Perrie,<sup>1</sup> and Yijun He<sup>2,3</sup>

Received 8 October 2009; revised 13 February 2010; accepted 25 February 2010; published 30 June 2010.

[1] C band RADARSAT-2 fully polarimetric (fine quad-polarization mode, HH+VV+HV+VH) synthetic aperture radar (SAR) images are used to validate ocean surface waves measurements using the polarimetric SAR wave retrieval algorithm, without estimating the complex hydrodynamic modulation transfer function, even under large radar incidence angles. The linearly polarized radar backscatter cross sections (RBCS) are first calculated with the copolarization (HH, VV) and cross-polarization (HV, VH) RBCS and the polarization orientation angle. Subsequently, in the azimuth direction, the vertically and linearly polarized RBCS are used to measure the wave slopes. In the range direction, we combine horizontally and vertically polarized RBCS to estimate wave slopes. Taken together, wave slope spectra can be derived using estimated wave slopes in azimuth and range directions. Wave parameters extracted from the resultant wave slope spectra are validated with colocated National Data Buoy Center (NDBC) buoy measurements (wave periods, wavelengths, wave directions, and significant wave heights) and are shown to be in good agreement.

**Citation:** Zhang, B., W. Perrie, and Y. He (2010), Validation of RADARSAT-2 fully polarimetric SAR measurements of ocean surface waves, *J. Geophys. Res.*, 115, C06031, doi:10.1029/2009JC005887.

### 1. Introduction

[2] Forecasts of ocean waves are crucial for ocean engineering and offshore structural design and navigation and for understanding and predicting severe marine weather. The satellite-borne synthetic aperture radar (SAR) is a powerful instrument to measure ocean waves at high resolution, with coverage over large areas, in almost any weather conditions. Measuring ocean waves from SAR can improve our understanding of upper ocean dynamics and help mitigate natural hazards. Presently, operational wave forecast models are driven by forecast winds and validated with in situ and remote sensing wave measurements. SAR wave measurements can improve wave forecasts.

[3] In recent years, considerable effort has gone into retrieving quantitative surface wave information from SAR images [Engen *et al.*, 1994; Plant and Zurk, 1997]. Data from several satellite missions, such as ERS-1, ERS-2, ENVISAT, and RADARSAT-1 have been used to estimate surface wave spectra from SAR images. Several different linear and nonlinear techniques [Lyzenga, 1988; Hasselmann and Hasselmann, 1991] have been developed for retrieving wave spectra from conventional single-polarization SAR

image spectra. However, the retrieval of a wave spectrum from an observed SAR spectrum with the nonlinear method requires a first guess wave spectrum from a numerical wave model. In order to avoid the dependence of the retrieved wave spectrum on the first guess wave spectrum, a semiparametric method was developed to retrieve a wave spectrum from an observed SAR image [Mastenbroek and de Valk, 2000]. The approach does not require a priori knowledge of sea state. Instead, each SAR image spectrum can be associated with a scatterometer wind vector; for ERS satellites, this is feasible since the scatterometer is operated simultaneously with the SAR. Unfortunately, this semiparametric method cannot retrieve wave spectra from ENVISAT, RADARSAT-1, or RADARSAT-2 images, because these satellites do not carry scatterometers. To solve the 180° ambiguity that exists inherently in ocean wave propagation, some ocean-SAR wave inversion methods using image cross spectra were proposed [Engen and Johnsen, 1995; Bao and Alpers, 1998; Dowd *et al.*, 2001]. Moreover, empirical and parametric inversion methods were developed for determination of time series of sea surface elevation maps from nautical radar image sequences [Dankert and Rosenthal, 2004] and for retrieval of integral ocean wave parameters from SAR image data [Schulz-Stellenfleth *et al.*, 2005, 2007], as well as extraction of ocean wave parameters from along-track interferometric SAR measurements [Zhang *et al.*, 2009].

[4] Conventional single-polarization backscatter cross-section measurements require two orthogonal passes and a complex SAR modulation transfer function (MTF) to determine vector slopes and directional wave spectra [Alpers *et al.*,

<sup>1</sup>Fisheries and Oceans Canada, Bedford Institute of Oceanography, Dartmouth, Nova Scotia, Canada.

<sup>2</sup>Institute of Oceanology, Chinese Academy of Sciences, Qingdao, China.

<sup>3</sup>Key Laboratory of Ocean Circulation and Waves, Chinese Academy of Sciences, Qingdao, China.

**Table 1.** RADARSAT-2 Fully Polarimetric Data Parameters for SAR Image Acquired on 25 February 2009

Radar Band	C Band
Radar center frequency (GHz)	5.40
Pulse repetition frequency (Hz)	2769.3
Satellite height (km)	795.8
Platform velocity (km/s)	7.46
Track angle (deg)	10.91
Slant range to velocity ratio (s)	137.6
Acquisition type	fine quad-polarization
Polarizations	HH VV HV VH
Raw data start time	2009-02-25T02:09:26.821106Z
Product format	GeoTIFF
Scene center	35°44'43"N 121°55'42"W
Incidence angle near range (°)	39.27
Incidence angle far range (°)	40.72
Sampled pixel spacing (m)	4.73
Sampled line spacing (m)	4.79

1981; *Hasselmann and Hasselmann*, 1991]. With the development of the fully polarimetric SAR technique, an algorithm was investigated to study the feasibility of using airborne L and P band fully polarimetric SAR image data to measure ocean wave slopes and wave spectra [*Schuler et al.*, 2004]. The advantage of this method is that it effectively achieves direct measurements of the wave slopes. The method was validated with Pacific swell observations under low-wind conditions. However, this method is only suitable for L or P band fully polarimetric SAR data, because it needs to estimate the polarization orientation angle, whereas C band data produce a very noisy polarization orientation angle image. Assuming the Bragg scattering model and Phillips wave spectrum, *He et al.* [2004] derived the tilt and polarization orientation modulation transfer functions of linear polarimetric SAR. Moreover, *He et al.* [2006] developed an approach to measure wave slope spectra using airborne C band fully polarimetric SAR data. However, cross-polarization information was not directly used, and this method was also only validated by using airborne SAR images.

[5] In this paper, we use C band RADARSAT-2 fully polarimetric SAR images to validate the polarimetric SAR wave retrieval algorithm proposed by *He et al.* [2006]. Copolarization and cross-polarization measurements are directly used when we retrieve wave slopes, and wave spectra and new validation results are presented. Retrieved wave parameters from the method are validated with collocated National Data Buoy Center (NDBC) buoy observations. Section 2 describes the data sets used, section 3 presents the wave retrieval methodology, and section 4 shows retrieved wave slopes and wave slope spectra. Conclusions are given in section 5.

## 2. Data Sets

[6] RADARSAT-2 is a relatively new Canadian C band spaceborne synthetic aperture radar, which was launched on 14 December, 2007. It supports all RADARSAT-1 beam modes, namely single-polarization standard, fine resolution, wide swath, ScanSAR, and extend coverage beams. Moreover, new modes include quad-polarization (HH+VV+HV+VH) imaging capabilities and multilook fine (which has the same resolution as fine resolution but uses four looks) and

ultrafine 3 m resolution models. All modes are available in both left- and right-looking orientations.

[7] In this study, we validate wave slopes and wave slope spectrum retrieval methods using six RADARSAT-2 fully polarimetric (quad-polarization mode) SAR images of various sea states and collocated National Data Buoy Center (NDBC) buoy data provided by the National Oceanic and Atmospheric Administration (NOAA). The quad-polarization modes provide fully polarimetric data, which means that complex images with each of four combinations of H and V on both transmit and receive are provided (HH, HV, VH, and VV). RADARSAT-2 quad-polarization products can be acquired in two different beam modes, namely fine quad-polarization and standard quad-polarization. Here, we use fine quad-polarization images to retrieve wave slopes and wave slope spectra. As an example, details regarding one of the six RADARSAT-2 fully polarimetric SAR images acquisition parameters are given in Table 1. The radar resolution cell has dimensions of 4.73 m (range direction) and 4.79 m (azimuth direction).

[8] NDBC data include observations from 6 m nondirectional buoys and 3 m discus wave directional buoys. A continuous set of hourly wind and wave parameters such as wind speeds, wind directions, significant wave heights ( $H_s$ ), and dominant wave periods ( $T_p$ ) are available from 6 m nondirectional buoys; the 3 m discus directional wave buoys provide mean wave directions. Studies show that the errors in the derived wave parameters from 3 m buoys are less than 3% in the significant wave heights and usually less than 4° in the peak wave direction [*Wang and Freise*, 1997]. We used measurements from three 3-m NDBC discus directional wave buoys (46028, 46029, and 46089) and two 6 m nondirectional NDBC wave buoys (46005 and 46071) for validations of the wave parameters estimated from SAR-retrieved wave slope spectra with in situ observations. These buoys are collocated with the six C band RADARSAT-2 fully polarimetric images. Information regarding the six SAR images and corresponding buoys are given in Table 2. Directional wave spectra, derived from the directional wave buoys,  $S(f, \theta)$  are represented, in the usual manner, as the products of the nondirectional wave height spectrum  $C_{11}(f)$  and the directional spreading functions  $D(f, \theta)$  as

$$S(f, \theta) = C_{11}(f)D(f, \theta), \quad (1)$$

$$D(f, \theta) = [1/2 + r_1 \cos(\theta - \theta_1) + r_2 \cos[2(\theta - \theta_2)]]/\pi, \quad (2)$$

where  $f$  is the wave frequency,  $\theta$  is the direction from which the wave arrives, measured clockwise relative to true north, according to the NDBC sign convention [*Steele et al.*, 1992],  $r_1$  and  $r_2$  are the first and second normalized (nondirectional) polar coordinates of the Fourier coefficients, and  $\theta_1$  and  $\theta_2$  are mean and principal wave directions, respectively.

[9] In some cases, it is necessary to transform the directional frequency spectrum  $S(f, \theta)$  to wave number spectrum  $S(k_x, k_y)$ . This transformation is done in two steps. First, the intermediate expression  $S(k, \theta)$  is expressed in terms of  $S(f, \theta)$  by

$$S(k, \theta) = S(f, \theta) \frac{df}{dk} = \frac{S(f, \theta)g}{8\pi^2 f} \left[ \tanh(kh) + \frac{kh}{\cosh^2(kh)} \right] \quad (3)$$

**Table 2.** RADARSAT-2 Fully Polarimetric SAR Image Data and NDBC Buoy Information

Image ID	Acquired Time (UTC)	Buoy Time	Image Central Site	Buoy Site	Wind Speed (m/s)	Wind Direction (°)
1	02:25:04 11 Jan 2009	02:50:00 11 Jan 2009	46°04'06"N 131°02'22"W	46°03'00"N 131°01'12"W	9.0	240
2	14:30:58 18 Jan 2009	14:50:00 18 Jan 2009	45°57'43"N 125°39'18"W	45°54'28"N 125°45'37"W	3.7	97
3	02:09:26 25 Feb 2009	01:50:00 19 Feb 2009	35°44'43"N 121°55'42"W	35°44'29"N 121°53'03"W	5.3	321
4	05:47:58 28 Feb 2009	05:50:00 28 Feb 2009	51°07'18"N 178°53'10"W	51°09'17"N 179°00'02"W	4.0	270
5	14:39:15 17 Mar 2009	14:50:00 17 Mar 2009	46°07'05"N 124°33'25"W	46°08'37"N 124°30'37"W	7.7	246
6	14:31:05 22 Aug 2009	14:50:00 22 Aug 2009	46°08'35"N 124°30'15"W	46°08'37"N 124°30'37"W	3.0	20

and  $S(k, \theta)$  can be expressed in terms of  $S(k_x, k_y)$  by using the Jacobian of  $(k, \theta)$  with respect to  $(k_x, k_y)$

$$S(k_x, k_y) = S(k, \theta) \frac{\partial(k, \theta)}{\partial(k_x, k_y)} = \frac{S(k, \theta)}{k} \quad (4)$$

where  $k$  is wave number,  $h$  is the finite water depth, and  $g = 9.81 \text{ m/s}^2$  is the gravitational acceleration.

### 3. Methodology

#### 3.1. Linearly Polarized Backscatter Cross Section

[10] For a SAR system that coherently transmits and receives both horizontal and vertical polarizations, the backscatter cross section  $\sigma(\chi, \psi)$  is determined for any arbitrary polarization state by calculating the Stokes matrix  $[M_{ij}]$  and the transmit and receive Stokes vectors according to

$$\sigma(\chi, \psi) = \frac{4\pi}{k_r^2} \begin{bmatrix} 1 \\ \cos(2\chi) \cos(2\psi) \\ \cos(2\chi) \sin(2\psi) \\ \sin(2\chi) \end{bmatrix}^T [M_{ij}] \begin{bmatrix} 1 \\ \cos(2\chi) \cos(2\psi) \\ \cos(2\chi) \sin(2\psi) \\ \sin(2\chi) \end{bmatrix} \quad (5)$$

where  $k_r$  is the transmitted radar wave number,  $T$  indicates a matrix transpose, and  $\chi$  and  $\psi$  are the ellipticity and polarization orientation angle, respectively. Equation (5) reduces to the horizontally polarized backscatter cross section when  $\chi = 0^\circ$  and  $\psi = 0^\circ$  and to the vertically polarized backscatter cross section when  $\chi = 0^\circ$  and  $\psi = 90^\circ$ .

[11] To obtain an expression for linearly polarized ocean backscatter cross sections, we utilize the scattering matrix  $[S_{ij}]$  for ocean polarization signatures, which is given as

$$S = \begin{bmatrix} S_{hh} & S_{hv} \\ S_{vh} & S_{vv} \end{bmatrix}. \quad (6)$$

Expressions for the terms  $[M_{ij}]$  of the Stokes matrix in terms of  $[S_{ij}]$  are well known [Van Zyl, 1985; Van Zyl et al., 1987]. For the scattering matrix of equation (6), the Stokes matrix  $[M_{ij}]$  reduces to the form

$$[M_{ij}] = \begin{bmatrix} M_{11} & M_{12} & M_{13} & M_{14} \\ M_{21} & M_{22} & M_{23} & M_{24} \\ M_{31} & M_{32} & M_{33} & M_{34} \\ M_{41} & M_{42} & M_{43} & M_{44} \end{bmatrix}, \quad (7)$$

where

$$\begin{aligned} M_{11} &= \frac{1}{4} [S_{hh} \cdot S_{hh}^* + S_{vv} \cdot S_{vv}^* + 2S_{hv} \cdot S_{hv}^*] \\ M_{12} &= \frac{1}{4} [S_{hh} \cdot S_{hh}^* - S_{vv} \cdot S_{vv}^*] \\ M_{13} &= \frac{1}{2} \Re [S_{hh} \cdot S_{hv}^*] + \frac{1}{2} \Re [S_{hv} \cdot S_{vv}^*] \\ M_{14} &= -\frac{1}{2} \Im [S_{hh} \cdot S_{hv}^*] - \frac{1}{2} \Im [S_{hv} \cdot S_{vv}^*] \\ M_{22} &= \frac{1}{4} [S_{hh} \cdot S_{hh}^* + S_{vv} \cdot S_{vv}^* - 2S_{hv} \cdot S_{hv}^*] \\ M_{23} &= \frac{1}{2} \Re [S_{hh} \cdot S_{hv}^*] - \frac{1}{2} \Re [S_{hv} \cdot S_{vv}^*] \\ M_{24} &= -\frac{1}{2} \Im [S_{hh} \cdot S_{hv}^*] + \frac{1}{2} \Im [S_{hv} \cdot S_{vv}^*] \\ M_{33} &= \frac{1}{2} S_{hv} \cdot S_{hv}^* + \frac{1}{2} \Re [S_{hh} \cdot S_{vv}^*] \\ M_{34} &= -\frac{1}{2} \Im [S_{hh} \cdot S_{vv}^*] \\ M_{44} &= \frac{1}{2} S_{hv} \cdot S_{hv}^* - \frac{1}{2} \Re [S_{hh} \cdot S_{vv}^*] \end{aligned}$$

and where  $\Re[\cdot]$  and  $\Im[\cdot]$  represent the real and imaginary parts of the indicated quantities, respectively. The remaining elements in the scattering matrix are determined by assuming that the matrix is symmetric.

[12] Because maximum sensitivities to wave slopes are obtained using only linear polarizations, the ellipticity ( $\chi$ ) is set to zero [Schuler and Lee, 1995]. We substitute equation (7) into equation (5), which yields a value for the linearly polarized backscatter cross section  $\sigma(0, \psi)$

$$\begin{aligned} \sigma(0, \psi) &= \frac{1}{4} (\sigma_{hh} + \sigma_{vv}) \cdot [1 + \cos^2(2\psi)] + \frac{1}{2} (\sigma_{hh} - \sigma_{vv}) \cos(2\psi) \\ &\quad + \sigma_{hv} + \frac{1}{2} \Re(\sigma_{hhvv}) \sin^2(2\psi), \end{aligned} \quad (8)$$

where  $\sigma_{hh}$ ,  $\sigma_{vv}$ ,  $\sigma_{hv}$ , and  $\sigma_{hhvv}$  are the radar backscatter cross sections for horizontal, vertical, cross polarizations, and the correlation between horizontal and vertical polarizations, respectively. Note that the equation (8) differs from the corresponding expressions derived by Schuler and Lee [1995] or He et al. [2006] by the additional term,  $\sigma_{hv}$ . Since RADARSAT-2 fully polarimetric (fine quad-polarization mode) SAR images provide copolarization (HH, VV) and

cross-polarization (HV, VH) measurements, we can use equation (8) and the polarization orientation angle ( $\psi$ ) to directly calculate the linearly polarized backscatter cross sections.

### 3.2. Wave Slopes in the Azimuth and Range Directions

[13] In the framework of linear modulation theory, the ocean surface elevation  $\xi$  and variations of the local backscatter cross section  $\sigma(\mathbf{r}, t)$  are remotely sensed by a real aperture radar. These may be represented as a superposition of propagating wave components, whose wave number is  $\mathbf{k}$  and frequency  $\omega$  are

$$\xi(\mathbf{r}, t) = \sum_k \xi_k \exp i(\mathbf{k} \cdot \mathbf{r} - \omega t) + c.c, \quad (9)$$

$$\sigma_{pp}(\mathbf{r}, t) = \bar{\sigma}_{pp} \left\{ 1 + \left[ \sum_k T_{kpp}^R \xi_k \exp i(\mathbf{k} \cdot \mathbf{r} - \omega t) + c.c \right] \right\}, \quad (10)$$

where  $\mathbf{r} = (x, y)$ ,  $x$  and  $y$  are component vectors in the radar look direction and platform flight direction, respectively. Here,  $\bar{\sigma}$  denotes the spatially averaged specific cross section, and  $c.c$  is the complex conjugate of the series.  $T_{kpp}^R$  is the real aperture radar (RAR) modulation transfer function, including tilt modulation  $T_{kpp}^t$ , hydrodynamic modulation  $T_k^h$ , polarization orientation angle modulation  $T_{kpp}^p$  [Lee *et al.*, 2000, 2002], and the range bunching modulation  $T_k^{rb}$ . Subscript “ $pp$ ” indicates the radar transmission and receiving polarizations, where  $p = h, v, \psi$  denote the horizontal, vertical, and linear polarizations, respectively, and the polarization orientation angle is given by  $\psi$ . For SAR, a velocity bunching modulation  $T_k^v$  must be included. Among all the modulations, only the tilt and polarization orientation angle modulation transfer functions depend on the radar polarizations. For conventional single polarization SAR (HH or VV), the velocity bunching modulation  $T_k^v$  must be included, whereas the polarization orientation angle modulation  $T_{kpp}^p$  produced by sea surface tilt [He *et al.*, 2004] vanishes when  $p$  represents horizontal or vertical polarizations. Therefore, equation (10) can be rewritten as

$$\frac{\Delta\sigma_{hh}(\mathbf{r}, t)}{\bar{\sigma}_{hh}} = \sum_k T_{khh}^t \xi_k \exp[i(\mathbf{k} \cdot \mathbf{r} - \omega t)] + c_1 + R, \quad (11a)$$

$$\frac{\Delta\sigma_{vv}(\mathbf{r}, t)}{\bar{\sigma}_{vv}} = \sum_k T_{kvv}^t \xi_k \exp[i(\mathbf{k} \cdot \mathbf{r} - \omega t)] + c_2 + R. \quad (11b)$$

For linearly polarized SAR with polarization orientation angle  $\psi$ , tilt and polarization orientation angle modulations exist at same time. Thus, equation (10) can be rewritten as

$$\frac{\Delta\sigma_{\psi\psi}(\mathbf{r}, t)}{\bar{\sigma}_{\psi\psi}} = \sum_k (T_{k\psi\psi}^t + T_{k\psi\psi}^p) \exp[i(\mathbf{k} \cdot \mathbf{r} - \omega t)] + c_3 + R, \quad (11c)$$

where  $R$  is given by

$$R = \sum_k (T_k^h + T_k^{rb} + T_k^v) \xi_k \exp[i(\mathbf{k} \cdot \mathbf{r} - \omega t)] + c_4, \quad (12)$$

where  $c_1, c_2, c_3, c_4$  are the complex conjugates of the series,  $T_{khh}^t$  and  $T_{kvv}^t$  are the tilt modulations for horizontal and vertical polarizations, respectively. Here,  $T_{k\psi\psi}^t$  and  $T_{k\psi\psi}^p$  are the tilt and polarization orientation angle modulations for the linear polarization with polarization orientation angle  $\psi$ , which are derived assuming a Bragg scattering model and Phillips wave spectrum [He *et al.*, 2006]. The polarization orientation angle modulation  $T_{k\psi\psi}^p$  is strictly a tilt effect and may be incorporated within the theory for tilt modulation. Here the rationale for separating it from the tilt modulation is the fact that existing ocean scattering theories generally do not develop the fully polarimetric scattering matrix amplitudes and phases [Schuler and Lee, 1995]. For equation (12),  $R$  includes hydrodynamic, range bunching, and velocity bunching modulations. There are no polarization-sensitive terms. Therefore we can obtain,

$$\frac{\Delta\sigma_{vv}(\mathbf{r}, t)}{\bar{\sigma}_{vv}} - \frac{\Delta\sigma_{hh}(\mathbf{r}, t)}{\bar{\sigma}_{hh}} = \sum_k (T_{kvv}^t - T_{khh}^t) \xi_k \exp i(\mathbf{k} \cdot \mathbf{r} - \omega t) + c_5, \quad (13a)$$

$$\frac{\Delta\sigma_{\psi\psi}(\mathbf{r}, t)}{\bar{\sigma}_{\psi\psi}} - \frac{\Delta\sigma_{vv}(\mathbf{r}, t)}{\bar{\sigma}_{vv}} = \sum_k (T_{k\psi\psi}^t + T_{k\psi\psi}^p - T_{kvv}^t) \xi_k \exp i(\mathbf{k} \cdot \mathbf{r} - \omega t) + c_6, \quad (13b)$$

where  $c_5$  and  $c_6$  are the complex conjugate of the series, respectively;  $T_{k\psi\psi}^t$  and  $T_{k\psi\psi}^p$  are given by equations (15a) and (15b) [see also He *et al.*, 2004] and

$$T_{kvv}^t = ik_x \frac{4 - 0.5(1 - \sin^2 \theta)}{\tan \theta(1 - \sin^2 \theta)}, \quad (14a)$$

$$T_{khh}^t = ik_x \frac{4 - 0.5(1 + \sin^2 \theta)}{\tan \theta(1 + \sin^2 \theta)}. \quad (14b)$$

Here  $\theta$  is the radar incidence angle, and  $k_x$  is the component of the incident wave number vector in the radar look direction.

[14] Inserting equations (14a) and (14b) and He *et al.* [2004, equations (15a) and (15b)] into equation (13), we perform straightforward algebraic calculations and obtain

$$\frac{\Delta\sigma_{vv}}{\bar{\sigma}_{vv}} - \frac{\Delta\sigma_{hh}}{\bar{\sigma}_{hh}} = -\frac{8 \tan \theta}{1 + \tan^2 \theta} \frac{\partial \xi}{\partial x}, \quad (15a)$$

$$\frac{\Delta\sigma_{\psi\psi}}{\bar{\sigma}_{\psi\psi}} - \frac{\Delta\sigma_{vv}}{\bar{\sigma}_{vv}} = A \frac{\partial \xi}{\partial x} + B \frac{\partial \xi}{\partial y}, \quad (15b)$$

where  $\partial \xi / \partial x$ ,  $\partial \xi / \partial y$  are wave slopes in the range and azimuth directions, respectively. Coefficients  $A$  and  $B$  in equation (15b) are also derived by He *et al.* [2006, equation (80)]. It is evident that wave slopes  $\partial \xi / \partial x$  and  $\partial \xi / \partial y$  can be obtained from equations (15a) and (15b) only when the polarization orientation angle ( $\psi$ ) is appropriately chosen. In He *et al.* [2006], cross-polarization information was not directly used when calculating the linearly polarized backscatter cross sections. Here copolarization (HH, VV) and cross-polarization (HV, VH) measurements are directly used to estimate linearly polarized backscatter cross sections and to retrieve wave slopes and wave spectra. The overall procedure for wave

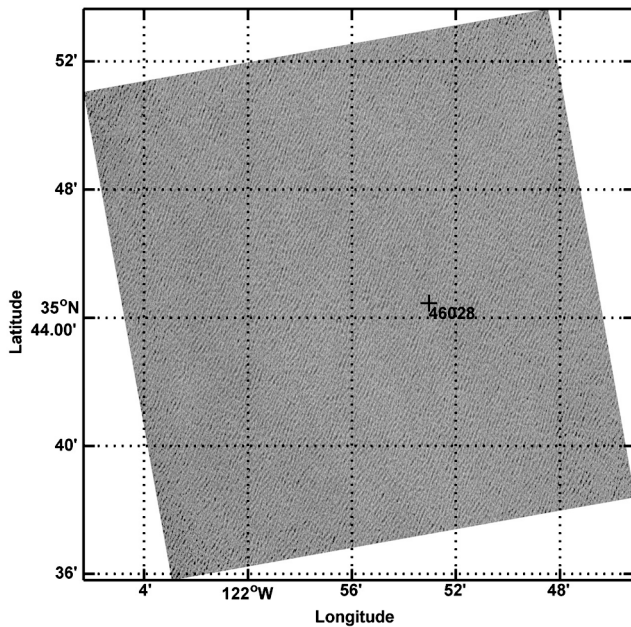


**Figure 1.** A C band, vertically (VV) polarized, image of area northwest of Morro Bay, CA acquired by RADARSAT-2 at 02:09 UTC on 25 February 2009. Further details are given in Tables 1 and 2. RADARSAT-2 Data and Products© MacDonald, Dettwiler and Associates Ltd. (2008–2009) – All Rights Reserved.

parameters extraction from RADARSAT-2 fully polarimetric SAR images can be summarized as follows:

[15] 1. Select  $512 \times 512$  pixel size HH-, VV-, and HV-polarized images, respectively, and transfer these slant range images into ground range images using linear interpolation in the range direction.

[16] 2. Estimate linearly polarized images using equation (8), which is the linear polarization  $p$ , when the polarization orientation angle  $\psi = 45^\circ$ .

[17] 3. Estimate the sea surface wave slope using equations (15a) and (15b) and smooth the slopes with a  $3 \times 3$  Gaussian filter.

[18] 4. Estimate wave slope spectrum, wavelength, wave direction, and wave height using wave slope images.

#### 4. Results and Analysis

[19] In this paper, six C band RADARSAT-2 fully polarimetric (fine quad-polarization mode) SAR images are used to retrieve ocean wave slopes and wave slope spectrum. These SAR images and colocated NDBC buoys are described in Table 2. All buoys are approximately located at the centers of the SAR images; the time intervals between RADARSAT-2 observations and buoy measurements are always less than 30 min. These are important factors in quantitative comparisons between retrieved wave parameters and buoy measurements. Figures 1 and 2 show C band RADARSAT-2 vertically (VV) polarized SAR images of an area northwest of Morro Bay, CA and an area northwest of Tillamook Bay, OR, respectively. Corresponding  $512 \times 512$  pixel size horizontally (HH) and vertically (VV) polarized images selected from these SAR images are presented in Figures 3a–3b and 4a–4b,

respectively. Figures 3c and 4c show the corresponding  $512 \times 512$  pixel size linearly polarized images, which are estimated from the HH, VV and cross-polarized (HV) images, and the polarization orientation angle ( $\psi = 45^\circ$ ). The wave slopes in azimuth and range directions calculated with these images are shown in Figures 3d, 3e, 4d, and 4e. We have applied a  $3 \times 3$  Gaussian filter to the wave slopes in order to eliminate noise. The retrieved wave slope spectra are shown in Figures 5 and 6, which can be directly used to extract estimates of the dominant wave lengths and wave directions.

[20] There is a  $180^\circ$  directional ambiguity in the SAR-retrieved wave slope spectra, since we did not use external information, such as first guess wave spectra from a wave model or wind observations from a scatterometer. We remove the directional ambiguity by using buoy-measured wave directions and wind directions. The dominant wavelengths are 242.9 and 245.2 m, with dominant propagation directions  $311.5^\circ$  and  $251.0^\circ$ , respectively, for the two cases shown in Figures 5 and 6. Figures 7 and 8 show the measured directional wave spectrum from NDBC buoys 46028 and 46089. The dominant wavelengths and propagation directions from the two buoys are 229.2 and 259.7 m and  $310.0^\circ$  and  $268.0^\circ$ , respectively.

[21] Figure 9 is a C band vertically (VV) polarized SAR image of an area west of Columbia River Mouth acquired under low-wind conditions; the dark areas correspond to the regions of very weak winds (3 m/s). A wave system is propagating with an estimated dominant wavelength of 193.9 m and a dominant wave direction of  $299^\circ$  (Figure 10).

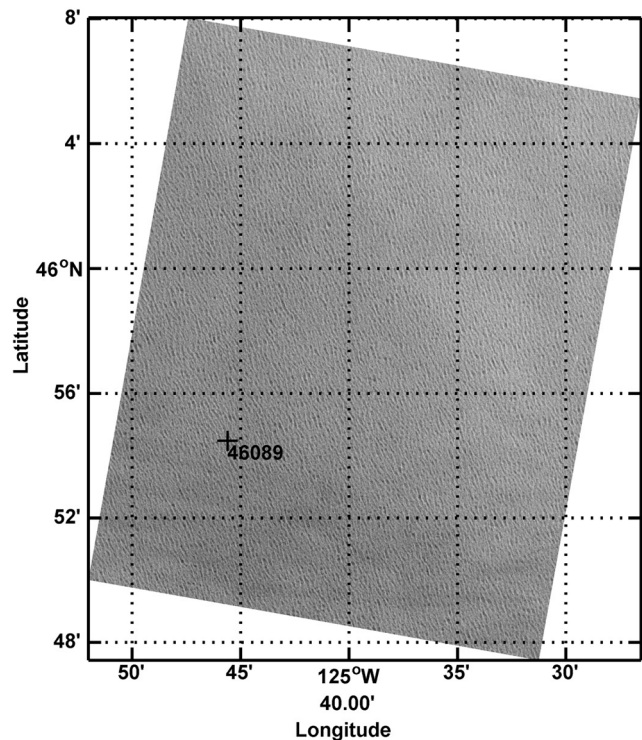


**Figure 2.** As in Figure 1, a C band, vertically (VV) polarized, image of area northwest of Tillamook Bay, OR acquired by RADARSAT-2 at 14:30 UTC on 18 January 2009. RADARSAT-2 Data and Products© MacDonald, Dettwiler and Associates Ltd. (2008–2009) – All Rights Reserved.

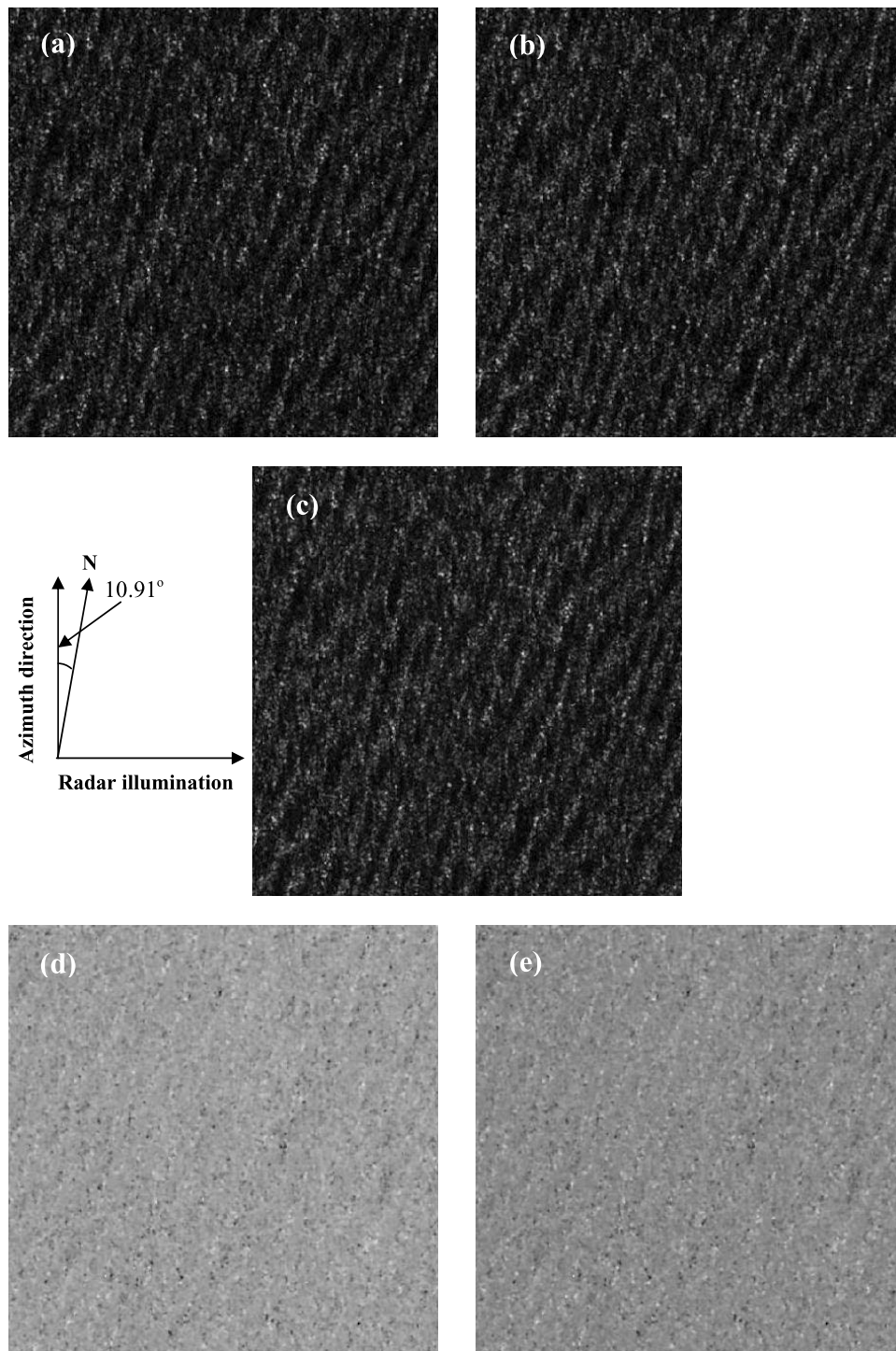


**Figure 3.** Corresponding  $512 \times 512$  pixel size images of area northwest of Morro Bay, CA selected from SAR image in Figure 1, at 02:09 UTC on 25 February 2009, showing (a) horizontal (HH) polarization, (b) vertical polarization, (c) linear polarization, (d) wave slope image in the azimuth direction, and (e) wave slope image in the range direction. NDBC directional wave buoy (46028) is collocated to these images.

The collocated measured wave spectrum from directional buoy 46029 is shown in Figure 11, with an estimated dominant wavelength of 188.8 m and wave direction of  $307^\circ$ .

[22] An additional interesting SAR image is shown in Figure 12, with retrieved wave spectrum in Figure 13. Here,

we can see a long period (15.57 s) swell, whose dominant wavelength and wave direction are 378.3 m and  $261.1^\circ$  (estimated from wave slope spectra in Figure 13). The collocated NDBC (46005) buoy-measured dominant wavelength and period are 399.5 m and 16 s, respectively.

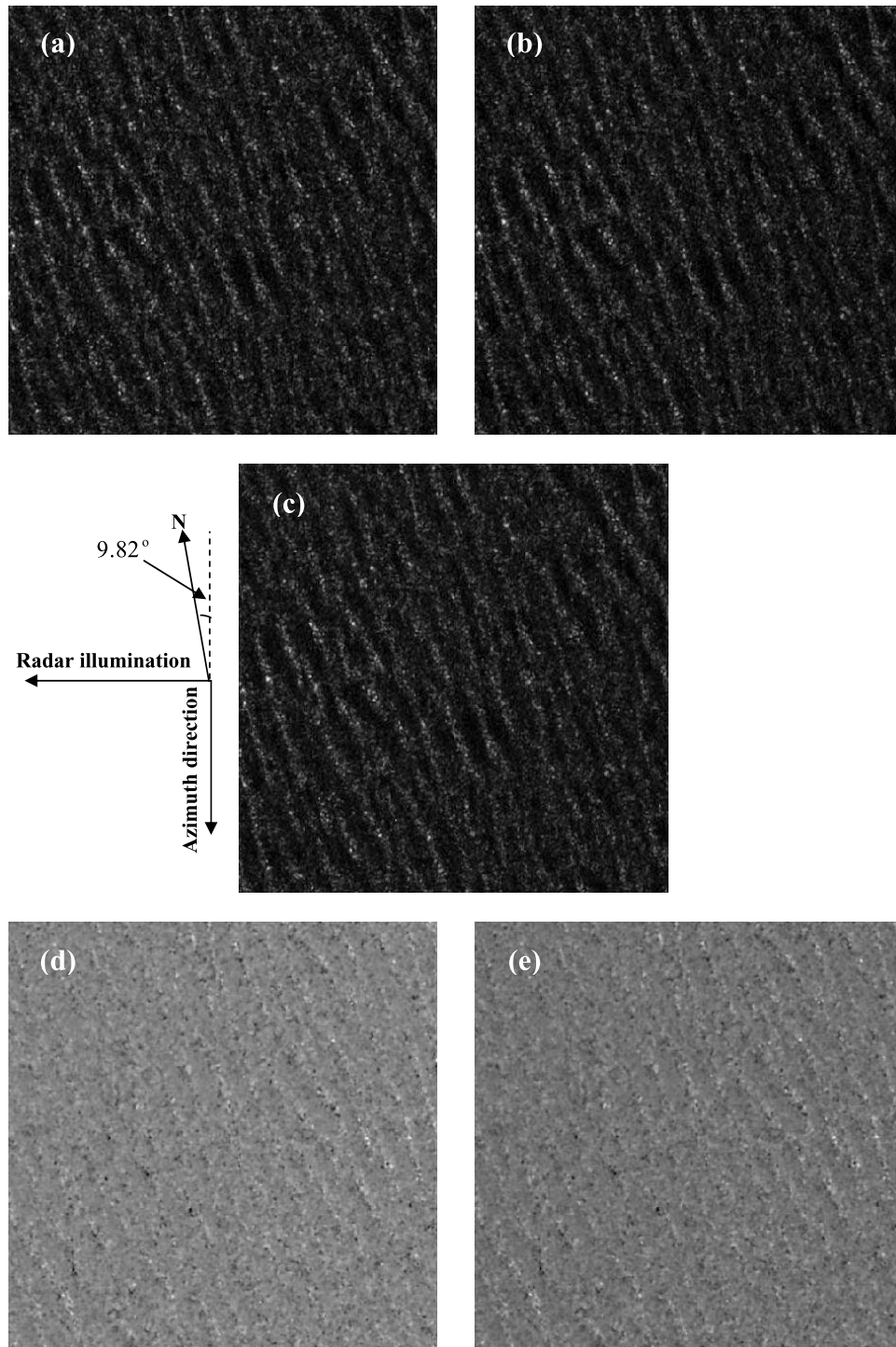


**Figure 4.** Corresponding  $512 \times 512$  pixel size SAR images of area northwest of Tillamook Bay, OR selected from SAR image in Figure 2, at 14:30 UTC on 18 January 2009, showing (a) horizontal (HH) polarization, (b) vertical (VV) polarization, (c) linear polarization, (d) wave slope image in the azimuth direction, and (e) wave slope image in the range direction. NDBC directional wave buoy (46089) is collocated to these images.

[23] We estimated the average wave heights of the dominant waves using the peak to trough root mean square (rms) slopes in the propagation directions  $S_{rms}$  and the dominant wavelengths  $\lambda_d$ . The estimated average dominant wave heights

( $H_d$ ) are then determined from  $\tan(S_{rms}) = H_d/(\lambda_d/2)$ . The rms slopes are calculated using the following relationship

$$S_{rms} = [(\langle S_{az} \sin \Phi \rangle)^2 + (\langle S_r \cos \Phi \rangle)^2]^{1/2}, \quad (16)$$

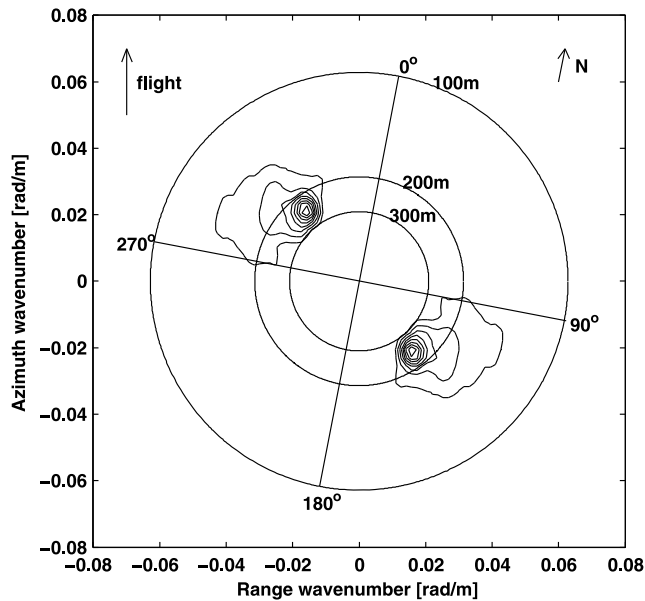


**Figure 5.** Wave slope spectrum from C band fully polarimetric SAR image of area northwest of Morro Bay, CA (Figure 1) acquired at 02:09 UTC on 25 February 2009.

where  $S_r = \partial\xi/\partial x$  and  $S_{az} = \partial\xi/\partial y$  are the wave slopes in the range and azimuth directions, respectively, and  $\Phi$  is the wave propagation direction. The rms slope  $S_{rms}$  is estimated over an ensemble of processed image pixels. Table 3 gives a comparison of SAR retrievals with buoy measurements for the estimated rms slopes, as well as the wave periods, wavelengths, wave directions, and significant wave heights. These results show good consistency between SAR-retrieved wave parameters and buoy data. Because the retrieved wave slope spectrum is a combination of wave slope spectrum in azimuth

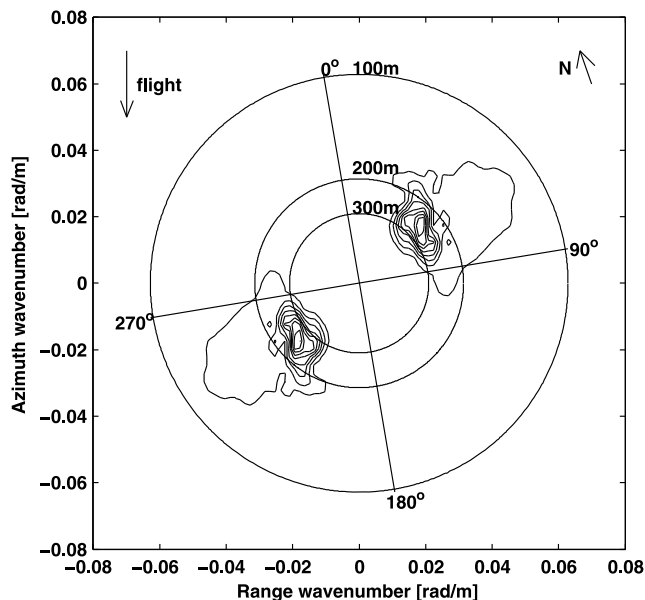


**Figure 6.** Wave slope spectrum from C band fully polarimetric SAR image of area northwest of Tillamook Bay, OR (Figure 2) acquired at 14:30 UTC on 18 January 2009.

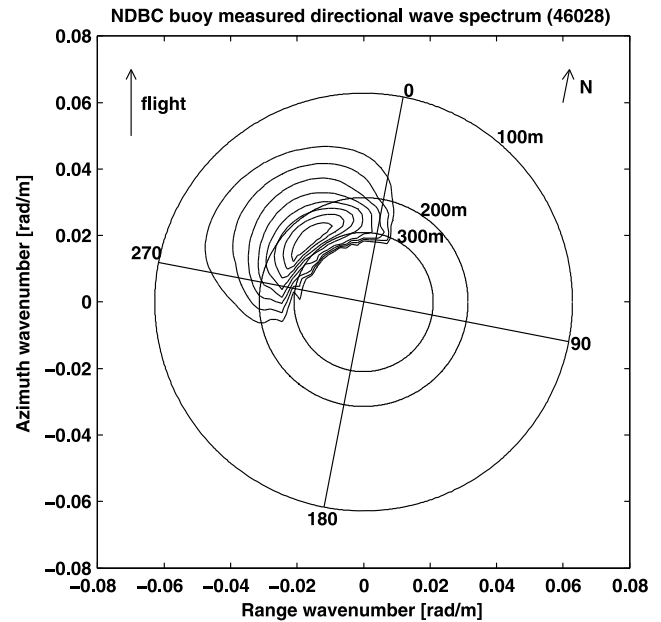


**Figure 7.** Directional wave spectrum measured by NDBC buoy (46028) colocating with the SAR image in Figure 1, at 01:50 UTC on 25 February 2009.

and range directions, it is not a complete wave slope spectrum and thus cannot be converted into a wave spectrum for comparisons with the buoy-derived spectrum.

### 5. Conclusions

[24] C band RADARSAT-2 fully polarimetric SAR images have been used to validate the polarimetric SAR wave retrieval algorithm proposed by *He et al.* [2006]. Ocean wave slopes in the azimuth and range directions can be directly

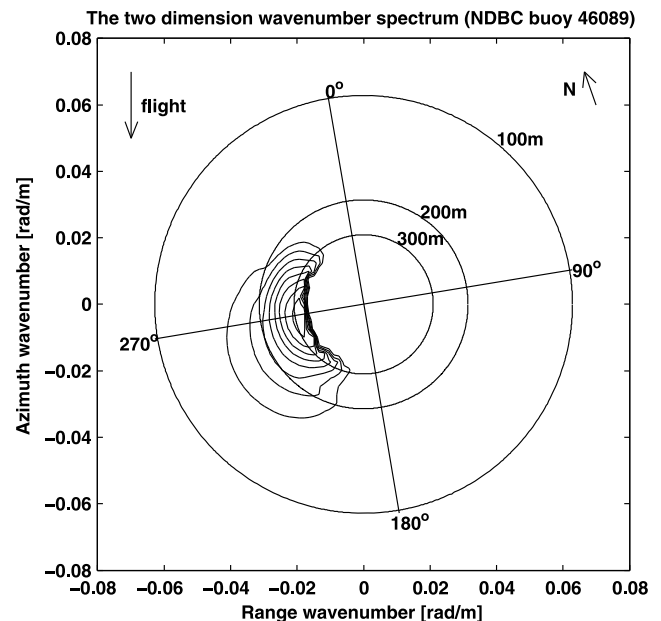


**Figure 8.** Directional wave spectrum measured by NDBC buoy (46089) colocating with the SAR image in Figure 2, at 14:50 UTC on 18 January 2009.

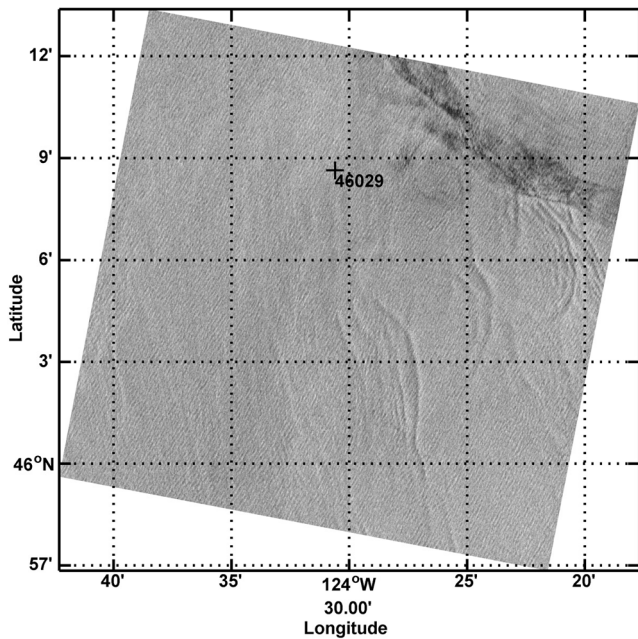


**Figure 9.** A C band, vertically (VV) polarized, image of area west of Columbia River Mouth acquired by RADARSAT-2 at 14:31 UTC on 22 August 2009. RADARSAT-2 Data and Products © MacDonald, Dettwiler and Associates Ltd. (2008–2009) - All Rights Reserved.

obtained using horizontally, vertically, linearly polarized backscatter cross sections, along with polarization orientation angle. The method does not require estimation of the complex hydrodynamic modulation function even under the large radar incidence angles. Wave parameters extracted from six RADARSAT-2 images are compared with in situ observations from NDBC buoys. The wavelengths, wave directions, significant wave heights, and wave periods are in good

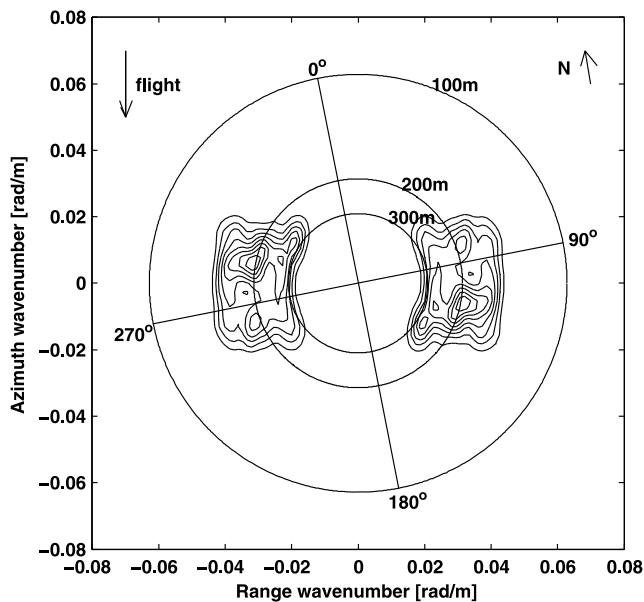


**Figure 10.** Wave slope spectrum from C band RADARSAT-2 fully polarimetric SAR image shown in Figure 9.

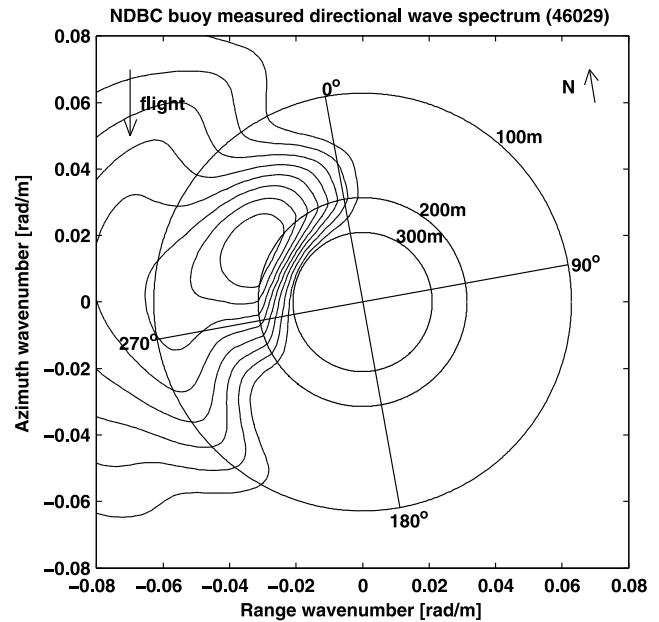


**Figure 11.** Directional wave spectrum measured by NDBC buoy (46029) at 14:50 UTC on 22 August 2009, colocating with SAR image in Figure 9.

agreement with those measured by buoys. Motion-related problems typical of SAR data, such as “velocity bunching” in the azimuth direction, must still be dealt with using iterative algorithms similar to those previously developed.

[25] There is a 180° directional ambiguity in the retrieved wave slope spectrum, since we do not use external informa-

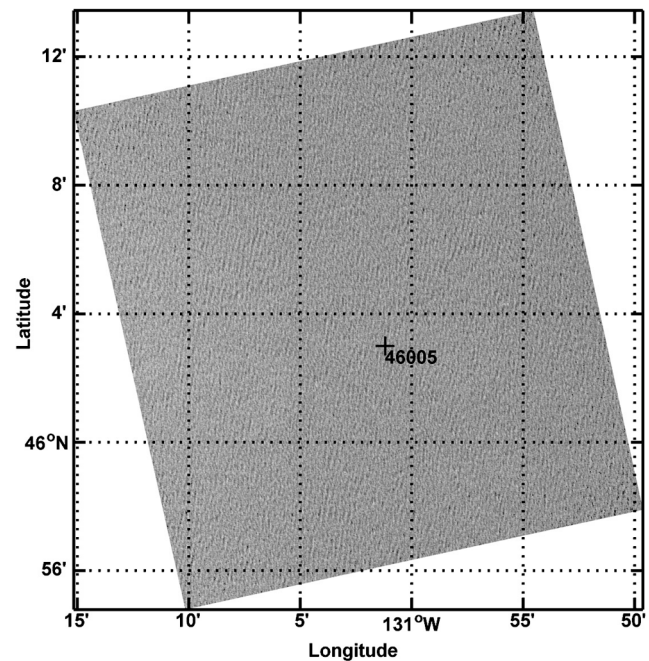


**Figure 12.** A C band, vertically (VV) polarized, image of area west of Aberdeen, WA acquired by RADARSAT-2 at 02:25 UTC on 11 January 2009. RADARSAT-2 Data and Products © MacDonald, Dettwiler and Associates Ltd. (2008–2009) - All Rights Reserved.

tion, such as first guess wave spectra from a numerical wave model or scatterometer wind data. We removed the directional ambiguity using the buoy-measured wave directions and wind directions. *He et al.* [2004] developed a simple method to eliminate the  $180^\circ$  directional ambiguity based on the fact that the polarimetric SAR image spectrum peaks are asymmetrical. However, this method is valid only at large incidence angles ( $>50^\circ$ ), which is not the case for RADARSAT-2 fully polarimetric SAR images because the associated incidence angles are between  $20^\circ$  and  $41^\circ$ . Alternately, the cross-spectrum method [*Engen and Johnsen, 1995*] can be used to remove the directional ambiguity for medium incidence angle cases.

[26] Additional research is needed to determine the extent to which the polarimetric SAR wave retrieval algorithm [*He et al., 2006*] is capable of measuring a more general wind-driven wave spectrum or a complex intersecting bimodal wave system. The polarimetric SAR wave retrieval algorithm is admittedly a linear retrieval technique and may thus produce errors under high sea state conditions, as it is well known that SAR image modulations are nonlinear under certain ocean surface conditions. As the sea state increases, the degree of nonlinear behavior will generally increase. Under these conditions, linear methods do not provide accurate quantitative estimates of the wave spectra [*Lyzenga, 1988*]. Thus, the method has limited utility to derive wave slopes and wave spectra under some conditions. The advantage of the method is that the RADARSAT-2 fully polarimetric SAR images can be directly used to extract wave parameters without estimating the complex hydrodynamic modulation transfer function. Moreover, other image intensity approaches, for example, the nonlinear inversion method [*Hasselmann and Hasselmann, 1991*], the cross-spectrum method [*Engen and Johnsen, 1995*], the semiparametric method [*Mastenbroek and de Valk, 2000*], or the parametric method [*Zhang et al., 2009*] need a hydrodynamic modula-

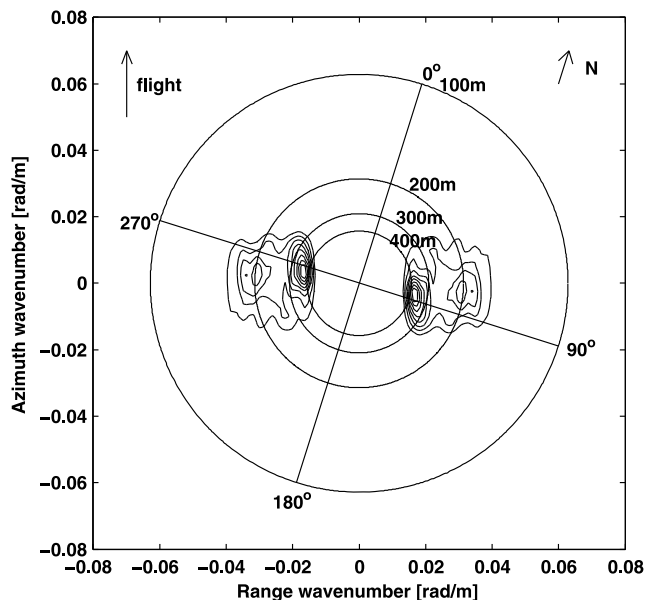


**Figure 13.** Wave slope spectrum from C band RADARSAT-2 fully polarimetric SAR image shown in Figure 12.

**Table 3.** Wave Parameters Extracted From the Six RADARSAT-2 Fully Polarimetric SAR (Fine Quad-Polarization Mode) Images in Table 2 Compared to Corresponding Wave Parameters Provided by NDBC Buoy Measurements

Parameter	Image ID	Buoy ID	Retrieval	Buoy
Wave period (s)	1	46005	15.57	16.00
	2	46089	12.54	12.90
	3	46028	12.48	12.12
	4	46071	11.51	11.00
	5	46029	12.89	12.90
	6	46029	11.15	11.00
Wavelength (m)	1	46005	378.3	399.5
	2	46089	245.2	259.7
	3	46028	242.9	229.2
	4	46071	206.7	188.8
	5	46029	259.2	258.8
	6	46029	193.9	188.8
Wave direction ( $^\circ$ )	1	46005	261.1	240.0
	2	46089	251.0	268.0
	3	46028	311.5	310.0
	4	46071	253.3	270.0
	5	46029	282.4	285.0
	6	46029	299.0	307.0
Significant wave height (m)	1	46005	2.91	3.10
	2	46089	2.67	2.51
	3	46028	2.74	2.88
	4	46071	4.08	4.10
	5	46029	2.98	3.44
	6	46029	2.08	2.50
RMS slope ( $^\circ$ )	1	46005	0.88	0.89
	2	46089	1.25	1.11
	3	46028	1.29	1.44
	4	46071	2.26	2.49
	5	46029	1.32	1.52
	6	46029	1.23	1.52

tion transfer function. However, the modulation transfer function is not well known. Moreover, when the radar incidence angle is about  $20^\circ$  for SAR wave mode data [i.e., for the ERS and ENVISAT], the hydrodynamic modulation transfer function is weak compared to the tilt modulation function and can be neglected. In this study, the incidence angles of the six RADARSAT-2 fully polarimetric images are larger than  $20^\circ$ . Therefore, the hydrodynamic modulation transfer function has to be estimated if one extracts wave parameters with these images using the other image intensity methodologies mentioned above. Here, the wave retrieval algorithm does not require estimation of the hydrodynamic modulation transfer function even though the radar incidence angle is larger than  $20^\circ$ , because it does not depend on the modulation function.

[27] **Acknowledgments.** The authors greatly appreciate the Canadian Space Agency for providing RADARSAT-2 fully polarimetric (fine quad-polarization mode) images. We wish to acknowledge NDBC for providing the buoy data products for validation of POLSAR wave retrieval algorithm. This work is partly supported by the Canadian Space Agency (CSA) GRIP project “Building Satellite Data Into Fisheries and Oceans Operational Systems,” and the CSA RADARSAT-2 project “Full polarization retrievals of ocean waves and winds”, and Chinese National High Technology Research and Development (863) Program (grant 2007AA12Z170), as well as the Knowledge Innovation Program of the Chinese Academy of Sciences (grant KZCX2-YW-201).

## References

- Alpers, W., D. B. Ross, and C. L. Rufenach (1981), On the detectability of ocean surface waves by real and synthetic aperture radar, *J. Geophys. Res.*, 86, 6481–6498.

- Bao, M., and W. Alpers (1998), On the cross spectrum between individual-look synthetic aperture radar images of ocean waves, *IEEE Trans. Geosci. Remote Sens.*, *36*, 922–932.
- Dankert, H., and W. Rosenthal (2004), Ocean surface determination from X band radar-image sequences, *J. Geophys. Res.*, *109*, C04016, doi:10.1029/2003JC002130.
- Dowd, M., P. W. Vachon, F. W. Dobson, and R. B. Olsen (2001), Ocean wave extraction from RADARSAT synthetic aperture radar inter-look image cross-spectra, *IEEE Trans. Geosci. Remote Sens.*, *39*, 21–37.
- Engen, G., and H. Johnsen (1995), SAR-ocean wave inversion using image cross spectra, *IEEE Trans. Geosci. Remote Sens.*, *33*, 1047–1056.
- Engen, G., H. Johnsen, and H. E. Krogstad (1994), Directional wave spectra by inversion of ERS-1 synthetic aperture radar ocean imagery, *IEEE Trans. Geosci. Remote Sens.*, *32*, 340–352.
- Hasselmann, K., and S. Hasselmann (1991), On the nonlinear mapping of an ocean wave spectrum into a synthetic aperture radar image spectrum and its inversion, *J. Geophys. Res.*, *96*, 10,713–10,729.
- He, Y., W. Perrie, T. Xie, and Q. Zhou (2004), Ocean wave spectra from a linear polarimetric SAR, *IEEE Trans. Geosci. Remote Sens.*, *42*, 2623–2631.
- He, Y., H. Shen, and W. Perrie (2006), Remote sensing of ocean waves by polarimetric SAR, *J. Atmos. Oceanic Technol.*, *23*, 1768–1773.
- Lee, J. S., D. L. Schuler, T. L. Ainsworth (2000), Polarimetric SAR data compensation for terrain azimuth slope variation, *IEEE Trans. Geosci. Remote Sens.*, *38*, 2153–2163.
- Lee, J. S., D. L. Schuler, T. L. Ainsworth, E. Krogager, D. Kasilingam, and W. M. Boerner (2002), On the estimation of radar polarization orientation shifts induced by terrain slopes, *IEEE Trans. Geosci. Remote Sens.*, *40*, 30–41.
- Lyzenga, D. R. (1988), An analytic representation of the synthetic aperture radar image spectrum for ocean waves, *J. Geophys. Res.*, *93*, 13,859–13,865.
- Mastenbroek, C., and C. F. de Valk (2000), A semiparametric algorithm to retrieve ocean wave spectra from synthetic aperture radar, *J. Geophys. Res.*, *105*, 3497–3516.
- Plant, W. J., and L. M. Zurk (1997), Dominant wave directions and significant wave heights from synthetic aperture radar imagery of the ocean, *J. Geophys. Res.*, *102*, 3473–3482.
- Schuler, D. L., and J. S. Lee (1995), A microwave technique to improve the measurement of directional ocean wave spectra, *Int. J. Remote Sens.*, *16*, 199–215.
- Schuler, D. L., J. S. Lee, D. Kasilingam, and E. Pottier (2004), Measurement of ocean surface slopes and wave spectra using polarimetric SAR image data, *Remote Sens. Environ.*, *91*, 198–211.
- Schulz-Stellenfleth, J., S. Lehner, and D. Hoja (2005), A parametric scheme for the retrieval of two-dimensional ocean wave spectra from synthetic aperture radar look cross spectra, *J. Geophys. Res.*, *110*, C05004, doi:10.1029/2004JC002822.
- Schulz-Stellenfleth, J., T. Köng, and S. Lehner (2007), An empirical approach for the retrieval of integral ocean wave parameters from synthetic aperture radar data, *J. Geophys. Res.*, *112*, C03019, doi:10.1029/2006JC003970.
- Steele, K. E., C.-C. Teng, and D. W. C. Wang (1992), Wave direction measurements using pitch-roll buoys, *Ocean Eng.*, *19*, 349–375.
- Van Zyl, J. (1985), On the importance of polarization in radar scattering problems, PhD. Thesis, Caltech Antenna Laboratory Report No. 120, California Institute of Technology, Pasadena, California.
- Van Zyl, J., H. A. Zebker, and C. Elachi (1987), Imaging radar polarization signatures: Theory and observations, *Radio Sci.*, *22*, 529–543.
- Wang, H. T., and C. B. Freise (1997), Error analysis of the directional wave spectra obtained by the NDBC 3-m pitch-roll disc buoy, *IEEE J. Oceanic Eng.*, *22*, 639–648.
- Zhang, B., W. Perrie, and Y. He (2009), Remote sensing of ocean waves by along-track interferometric synthetic aperture radar, *J. Geophys. Res.*, *114*, C10015, doi:10.1029/2009JC005310.
- Y. He, Institute of Oceanology, Chinese Academy of Sciences, Qingdao, 266071, China.
- W. Perrie and B. Zhang, Fisheries and Oceans Canada, Bedford Institute of Oceanography, 1 Challenger Dr., P O Box 1006, Dartmouth, NS B2Y 4A2, Canada. (perriew@dfo-mpo.gc.ca)